Three-body kinematical correlation in the dissociative recombination of CH_2^+ by three-dimensional imaging

I. Nevo,[1] S. Novotny,[2] H. Buhr,[2] V. Andrianarijaona,[2] S. Altevogt,[2] O. Heber,[1] J. Hoffmann,[2] H. Kreckel,[2] L. Lammich,[2] M. Lestinsky,[2] H. B. Pedersen,[2] D. Schwalm,[1,2] A. Wolf,[2] and D. Zajfman[1,2]
[1]*Department of Particle Physics, Weizmann Institute of Science, Rehovot, 76100, Israel*
[2]*Max-Planck-Institut für Kernphysik, D-69117 Heidelberg, Germany*
(Received 24 April 2007; published 29 August 2007)

A three-dimensional imaging technique installed at the Heidelberg Test Storage Ring (TSR) has been used to investigate the three-body breakup channels occurring in the dissociative recombination process of the methylene ion CH_2^+. By selecting dissociation planes perpendicular to the molecular beam direction the dissociation kinematics could be measured with unprecedented momentum resolution. Release energies, the relative branching ratio, and the kinematical correlations between the three fragments were determined for the two energetically allowed channels: $C(^3P)+H(^2S)+H(^2S)$ and $C(^1D)+H(^2S)+H(^2S)$.

DOI: 10.1103/PhysRevA.76.022713 PACS number(s): 34.80.Ht, 33.15.Bh, 33.15.Vb

I. INTRODUCTION

In dilute plasmas which are cold enough to contain molecular ions, dissociative recombination (DR) is the dominant process for removing electrons. The process is thereby not only controlling the amount of ionization in these media, it also constitutes an important loss channel for molecular ions and a source of energetic neutral atoms and excited molecules. DR rates, branching ratios, and the energy sharing between inner and outer degrees of freedom of the fragments are thus important ingredients in modeling these plasmas.

Even though the basic principle of DR has been known for more than 50 years [1] and a close to quantitative understanding of the DR of diatomic molecular ions has been achieved in the meantime [2], the theoretical description of the DR process of polyatomic ions is still in its infancy; only recently theory succeeded in reproducing the measured DR rate for the simplest three-atom system H_3^+ [3], one of the main difficulties being caused by the two-dimensionality of the process. On the experimental side, considerable progress has been made since the advent of heavy-ion storage rings with merged electron beams, which do allow one to control the inner excitation of the molecular ions and the relative ion-electron energy precisely enough to produce data in the parameter space of interest for, e.g., planetary atmospheres or interstellar chemistry [4], and accessible to theoretical considerations. Despite these experimental advances, in particular in the study of diatomic systems, detailed investigations of the DR process for polyatomic ions, such as measurements of branching ratios at relative energies other than zero, of the inner excitation of neutral molecular fragments, of angular distributions, or of the dissociation kinematics are still limited by the presently available detection techniques for DR reaction products.

Recently, we have installed a three-dimensional (3D) imaging system at the Heidelberg Test Storage Ring (TSR) [5], which is based on the concept of Strasser *et al.* [6] and allows one to measure all three velocity components of the DR fragments and thus provides experimental access to study the dissociation kinematics of polyatomic molecular ions. In dissociative recombination the released energy is transferred to translational degrees of freedom of the products and to their internal excitation. For diatomic molecules, the way in which the energy is shared between the two fragments is fixed by energy and momentum conservation. For DR reactions of polyatomic molecules that yield three or more fragments, however, the energy and momenta restrictions alone do not determine uniquely the dissociation kinematics, but the final magnitudes and relative directions of the fragments momenta are influenced by the dissociation dynamics as well. Previously, the dissociation kinematics of the DR products of the triatomic molecular ion, H_3^+, and its isotopomers, D_3^+, H_2D^+, and D_2H^+, at zero relative ion-electron energies could be studied at the TSR by 2D imaging of the two- and three-body dissociation channels [7], i.e., by measuring only transversal velocities of the fragments. In these specific cases, the presence of only one dissociation channel with three fragments, sharing a single fixed kinetic energy release, permitted us to extract the dissociation kinematics by 2D imaging alone. In general, however, the use of 2D imaging for inferring the dissociation geometries of three-body and higher multiplicity DR reactions is severely restricted if not impossible; the measurement of all three velocity components of the fragments is required to be able to access this information.

In the present paper, we report on our first measurement of the three-body breakup of a triatomic molecular ion using the new 3D imaging system. Even though the time resolution of the system and thus the resolution for the longitudinal fragment velocities was not yet optimal at the time of the experiment, we could separate the different three fragment channels and determine uniquely their kinematical properties as well as their relative branching ratios. The study was performed for the methylene cation CH_2^+, where the DR at zero relative electron-ion energy leads to two three-fragment channels

$$CH_2^+(\tilde{X}^2A_1) + e^- \rightarrow C(^3P) + H(^2S) + H(^2S)$$
$$\rightarrow C(^1D) + H(^2S) + H(^2S).$$

Several reasons prompted us to choose the CH_2^+ ion for this

feasibility study: Experimentally, the two three-fragment channels are known [8] to account for about 63% of all DR events, and they are expected to be well distinguishable in view of their different release energies. Moreover, Thomas *et al.* [9,10] reported recently about experimental DR results for a series of three atomic molecular ions, including the methylene ion. Based on a special 2D imaging technique, they determined the relative branching ratios between the two three-fragment channels of CH_2^+, and obtained information on the kinetic energy releases as well as on the preferred dissociation geometry, results to which the present experimental findings can be readily compared. Moreover, CH_2^+ plays a central role in the chemistry of dense and diffuse interstellar clouds [4], where it is believed to be the nucleus for forming larger hydrocarbon ions through reactions involving neutral hydrogen molecules. The DR process of hydrocarbon ions is thus an important cornerstone in all astrochemical networks. As long as no reliable theoretical descriptions of the DR process of polyatomic molecular ions are available, the required input data still has to come from experiment, but the increasing availability of detailed experimental data on the DR process is hopefully also stimulating and guiding further theoretical developments.

II. EXPERIMENTAL PROCEDURE

A. Experimental setup

The experiments presented here were carried out at the Test Storage Ring (TSR) of the Max-Planck-Institut für Kernphysik in Heidelberg, Germany. A beam of 6.68 MeV CH_2^+ ions was formed in the stripper gas channel located in the terminal of a tandem Van de Graaf accelerator by fragmentation of a primary 4.7 MeV CH_3O^- ion beam, which was produced by a sputter source. The ions were injected into the storage ring and kept circulating for up to 11 s at a residual background gas pressure of 3×10^{-11} mbar.

During storage, the ions were continuously subjected to the influence of an electron beam produced by the thermal cathode of the TSR electron target [11]. The electrons were copropagating with the ions over an effective distance of $\sim$1.25 m at zero average relative velocity. Thereby the ion beam was phase-space cooled within $\sim$2 s and kept cold during the course of the subsequent DR measurements. The transversal and longitudinal temperature of the electrons was $kT_\perp=3.7$ meV and $kT_\parallel=58$ μeV, respectively, while the electron density was chosen to be between 6×10^6 cm^{-3} and 2×10^7 cm^{-3}. For some runs the electron cooler, located in a different quadrant of the TSR, was used in addition to speed up phase-space cooling. Depending on the actual cooling times reached only events recorded after a storage time of $>2-3$ s have been considered in the final data analysis. As shown in Coulomb explosion imaging measurements on CH_2^+ [12], this time cut also ensures that all molecules have quantitatively relaxed to the vibrational ground state, while remaining excitations of the ground state rotational bands are expected to reach full equilibrium with the 300 K background radiation only at the end of the measuring cycle.

Neutral fragments of the molecular CH_2^+ ion that underwent a DR process in the interaction region of the electron target (energy in the ion-electron center of mass system $E_{\mathrm{c.m.}}=0\pm^{3.7}_{0.0}$ meV) were detected downstream of the electron target by the new 3D fragment-imaging setup located at a distance of 12.24 m from the center of the interaction region. The 3D detector consists of a 80 mm diameter Chevron microchannel plate (MCP) coupled to a fast phosphor screen [P-47 (Y_2SiO_5:Ce), decay time $\tau=54$ ns], which is faced by two charge-coupled device (CCD) cameras, one of which is equipped with a fast optical shutter. For a detailed description of this new 3D imaging technique the reader is referred to Refs. [5,6]. Briefly, the lateral impact positions of the DR fragments on the MCP plane are derived as usual from the position of the light spots observed by the nongated CCD camera, which is integrating the fluorescence light emitted from each spot over a long time compared to the characteristic decay time τ of the phosphor screen. In contrast, the light integration of the gated CCD camera is stopped after a fixed gating time t_g, which is started by the fragment arriving first at the MCP. Thus, in case t_g is short compared to τ, the spot intensity measured by the gated CCD camera, normalized to the total spot intensity as determined by the nongated camera, is a measure of the impact time difference of the fragment with respect to the fastest one. As the velocity of the center of mass is known (in the present experiment the beam velocity), the setup thus allows us to determine all three velocity components of the fragments.

The two CCD cameras were synchronized and read out at a frame rate of 30 Hz. As the number of events recorded by the MCP were of the order of 1 kHz, the phosphor screen was operated in a trigger mode, switching off the acceleration voltage between the MCP and the screen within $\sim$5 μs after an event was seen by the MCP. In this way, the probability of observing two independent events within one frame could be kept in the range of a few percent.

B. Data analysis

The data was first sorted according to the number of distinguishable light spots recorded simultaneously in both the gated and ungated CCD camera using a peak finding routine. The minimum distance between two spots was $\sim$5 mm. The transversal (x_i, y_i) coordinates of each fragment were then deduced from the light spots observed by the nongated CCD camera with an accuracy of $\sim$150 μm. The pixel-to-mm conversion was determined by means of a metal plate with a set of holes 10 mm apart, which was placed during one measurement in front of the MCP, the accuracy of the conversion factors being $\pm1\%$. The mass assignment of the three fragments following the DR of CH_2^+ was performed in the usual way by calculating the (transversal) center of mass (c.m.) of the event for all three possible permutations and selecting the mass assignment resulting in a c.m. being closest to the beam center. In a second step, the transversal coordinates of the three fragments with respect to the c.m. of the event are derived, restricting the further analysis to frames with c.m. within a distance $R_{\mathrm{c.m.}}\leq\sigma_R$ from the beam center, σ_R being the variance of the c.m. distribution around the beam center. Finally, the total projected distance D is calculated by

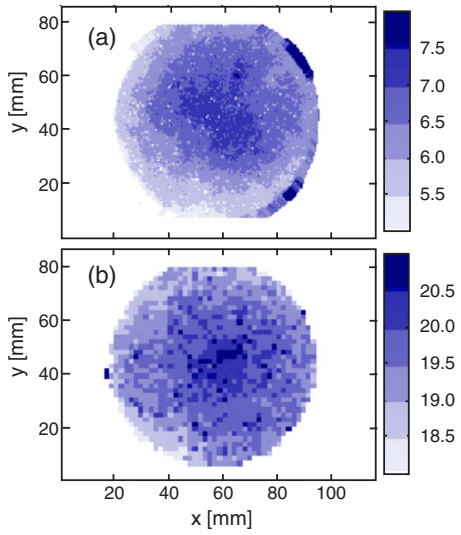

FIG. 1. (Color online) (a) The calibration function $k(x,y)$ derived from a measurement of $\tilde{\Omega}_i$ for $(t_g-t_i)\to\infty$. (b) The effective trigger time $t_g(x,y)$ (in ns) derived from one-spot frames.

$$D=\sqrt{d_{\mathrm{H}_1}^2+d_{\mathrm{H}_2}^2+\frac{m_{\mathrm{C}}}{m_{\mathrm{H}}}d_{\mathrm{C}}^2}, \tag{1}$$

where m_{H} and m_{C} denote the mass of the hydrogen and carbon atoms, respectively, and d_{H_1}, d_{H_2}, and d_{C} are their transversal distances from the molecular c.m. The projected distance D is connected to the transversal total kinetic energy release $E_\perp$ by

$$E_\perp=E_B\frac{m_{\mathrm{H}}}{M}\frac{D^2}{s^2}, \tag{2}$$

for an event occurring at a distance s from the imaging detector, with $M=2m_{\mathrm{H}}+m_{\mathrm{C}}$ and E_B being the laboratory energy of the circulating ion beam.

The impact time t_i of the ith fragment on the MCP is determined from the ratio $\tilde{\Omega}_i$ of the integrated intensities I_i^g and I_i^n as recorded for the ith light spot by the gated and nongated CCD camera, respectively. Assuming the light curve of the phosphor screen to be exponential, this ratio is given by (see also Ref. [6])

$$\tilde{\Omega}_i\equiv\frac{I_i^g}{I_i^n}=k[1-e^{(t_i-t_g)/\tau}], \tag{3}$$

where k takes into account the different sensitivities of the gated and the nongated CCD camera. To determine k under experimental conditions a measurement was performed setting $(t_g-t_i)\to\infty$. Practically, the construction of the k function was implemented by exposing the gated camera to light emitted from the phosphor screen for times ($\sim$10 μs) that are much longer than τ. In this way, for each position (x,y) on the phosphor screen k has been determined, which resulted in the distribution shown in Fig. 1(a). Moreover, the effective gating time t_g was determined analyzing those frames taken during the production runs, which contain only one impact. These single particle frames are mainly caused by the finite efficiency of the MCP and by fragments from breakup reactions of the circulating molecules on the TSR rest gas. As for these frames the electronic gate is started by the fragment itself, $t_i=0$, and Eq. (3) results in

$$t_g=-\tau\ln\left(1-\frac{\tilde{\Omega}_1}{k}\right). \tag{4}$$

A typical t_g distribution obtained in this way is shown in Fig. 1(b).

While the observed variation of k with the light spot position can be readily explained to be caused by various experimental imperfections of the CCD cameras and of the image intensifier used as an optical shutter, the discussion of the origin of the position dependence of t_g is more intricate. The (x,y)-dependence of t_g, which amounts to 1.5 ns when comparing the central area of the detector, mainly hit by carbon fragments, to the outer areas hit by the hydrogen atoms, can be due to at least three causes: A position (intensity, rate) dependence of (i) the electronic trigger derived from the MCP, (ii) the actual closing time of the shutter, and (iii) the decay time of the phosphor screen. As we are finally only interested in the impact time difference, which is independent of the time the electronic trigger has been started, effects due to (i), while influencing the single particle frame analysis, would drop out in the analysis of the DR measurements. By performing the DR analysis assuming (a) the total variation being due to (i), and (b) the effects being solely due to (ii) and (iii), it turns out that only procedure (b) results in symmetric distributions of the impact time differences. The impact time difference between two of the fragments was therefore deduced by

$$\Delta t_{i,j}=t_i-t_j=\tau\ln\left(\frac{1-\frac{\tilde{\Omega}_i}{k(i)}}{1-\frac{\tilde{\Omega}_j}{k(j)}}\right)+t_g(i)-t_g(j), \tag{5}$$

properly smoothing the measured $k(x,y)$ and $t_g(x,y)$ distributions to avoid statistical artifacts.

The $\Delta t_{\mathrm{H,C}}$ distribution resulting from the DR of CH_2^+ into the three-fragments channels is shown in Fig. 2, each event contributing two entries to the histogram. For symmetry reasons the graph is required to be reflection symmetric around $\Delta t_{\mathrm{H,C}}=0$, which is indeed fulfilled if the t_g correction is applied as discussed above. Also shown is the result of a Monte Carlo simulation assuming the time resolution for the individual impact times t_i to be $\sigma_t=0.9$ ns. Comparing σ_t to the maximum time-of-flight difference of $\sim$6 ns, it is obvious that the time resolution achieved is not yet sufficient to allow for a detailed three-dimensional analysis of the dissociation kinematics of CH_2^+. To reach an optimal time resolution the gating time should be only slightly larger than the maximum time-of-flight difference of the fragments. At the time of the present experiment, however, the shortest gating time that could be realized was $t_g\sim 20$ ns [compare Fig. 1(b)], which was mainly determined by the transient time of the trigger pulse through the electronics. We are presently implementing a delay line for the light seen by the gated camera [5], which will allow us to optimize the integration time with respect to the flight time differences in future experiments.

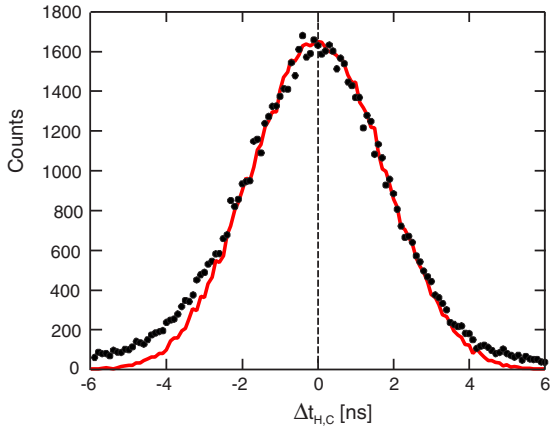

FIG. 2. (Color online) The measured time distribution $\Delta t_{H,C} = t(H) - t(C)$ (solid points). The solid (red) line is the result of a MC simulation assuming a time resolution of $\sigma_t = 0.9$ ns. The simulated curve was adjusted to the height of the measured distribution around $|\Delta t_{H,C}| = 0$ ns.

In view of the limited time resolution reached in the present experiment, the time information was only used in the following analysis to select DR events where the normal of the molecular plane was oriented parallel to the beam direction. For this purpose the angle θ between the beam axis and the normal of the molecular plane was calculated event by event from the measured c.m. velocities of the three fragments. A histogram of the number of DR events as a function of $\cos(\theta)$ is plotted in Fig. 3 together with the result of a Monte Carlo simulation. Only DR events were considered which fulfilled, in addition to the already mentioned conditions, the time cut $|\Delta t_{H,C}| \leq 6$ ns for both H. The dip in the distribution around $\cos(\theta) \sim 0$ is due to an efficiency loss caused by the time cut for these orientation angles, which does not seem to be properly simulated by assuming a Gaussian time resolution function (see also Fig. 2). If not otherwise stated, only events with $|\cos(\theta)| \geq 0.8$ were considered in the following analysis of the 3D-imaging data. This

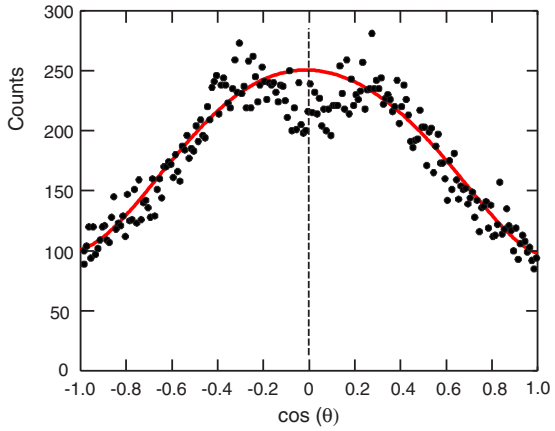

FIG. 3. (Color online) Measured distribution of the orientation angle θ between the normal of the dissociation plane and the ion beam direction for events with $|\Delta t_{H,C}| < 6.0$ ns (solid points). The MC simulation assuming a time resolution of $\sigma_t = 0.9$ ns is shown by the solid (red) line (see also main text).

cut reduces considerably the data sample, but by selecting dissociation planes perpendicular to the beam direction the three-dimensional kinematic is approximately reduced to a two-dimensional, transversal one, where advantage can be taken of the better transversal momentum and energy resolution.

C. Monte Carlo simulations

All analysis steps are accompanied by detailed Monte Carlo (MC) simulations that mimic the dissociation process. The simulations include the following assumptions and steps: (i) The dissociation planes are isotropically oriented, and the individual momenta of the fragments—if not otherwise stated—are randomly distributed in the Dalitz circle (see Sec. III A). (ii) The kinetic energy release E_k for the $C(^1D)$ channel with respect to the rovibrational ground state of CH_2^+ is fixed to that of the $C(^3P)$ channel by $E_k(^1D) = E_k(^3P) - 1.264$ eV [13]. Moreover, if not varied, $E_k(^3P)$ and the $[C(^3P)]:[C(^1D)]$ branching ratio are taken to be 2.62 eV and 68:32, respectively. (iii) A rotational excitation of the ground vibronic state [14] is assumed according to a Maxwell-Boltzmann distribution for a temperature of 300 K. (iv) The dissociation occurs randomly and uniformly in the interaction region (effective length 1.25 m; mean distance to the imaging detector $s_0 = 12.24$ m). (v) The dissociation events are generated having molecular c.m., which are normally distributed around the beam center with a standard deviation that typifies the measured c.m. distribution. Moreover, the time-of-flight of each fragment is chosen to be normally distributed with a standard deviation σ_t.

The simulated events are finally subjected to the same algorithm used to analyze the measured data.

III. RESULTS

A. Dissociation kinematics

For DR channels leading to three fragments, the dissociation kinematics can be represented in a concisive way by using the two-dimensional representation (η_1, η_2) introduced by Dalitz [15]. In the case of the three-body DR of $CH_2^+ + e^-$, which results in two identical hydrogen fragments, the two Dalitz coordinates (η_1, η_2) are conveniently defined by

$$\eta_1 = \sqrt{\frac{M}{3m_C}} \frac{E_{H_2} - E_{H_1}}{\sqrt{3}E}, \qquad \eta_2 = \frac{M}{3m_H} \frac{E_C}{E} - \frac{1}{3},$$

where E_H and E_C are the c.m. energies of the individual fragments and $E = E_{H_1} + E_{H_2} + E_C$ denotes the total kinetic energy release. Each point in the Dalitz plane, which is confined by a circle of radius 1/3 imposed by the energy and momentum conservation, uniquely defines the energy sharing and hence the momenta of the fragments. An alternative representation of the dissociation kinematics is given by the two c.m. angles χ_D and ξ_D, with $\chi_D = \angle(\vec{p}_{H_1}, \vec{p}_{H_2})$ denoting the c.m. angle between the final momenta of two H atoms and $\xi_D = \angle(\vec{p}_{H_>}, \vec{p}_C)$ describing the c.m. angle between the hydrogen with the larger momentum and the final momentum of the carbon fragment. The correspondence between

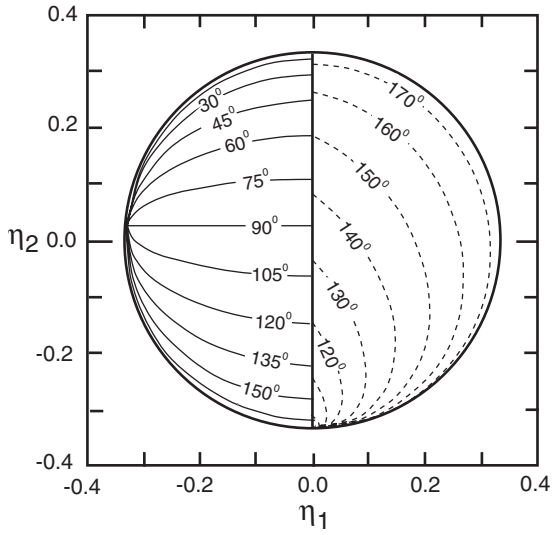

FIG. 4. Dalitz plot for three-body final channel following the DR of CH_2^+, depicting the correspondence between the Dalitz coordinates (η_1, η_2) and the c.m. angles $\chi_D = \angle(\vec{p}_{H_1}, \vec{p}_{H_2})$ (solid lines in the left half circle) and $\xi_D = \angle(\vec{p}_{H_>}, \vec{p}_C)$ (dashed lines in the right half circle), with $H_>$ denoting the hydrogen with the larger momentum. Note that the Dalitz plot is symmetric around $\eta_1 = 0$.

(χ_D, ξ_D) and the (η_1, η_2) coordinates is shown in Fig. 4, taking advantage of the symmetry of the Dalitz plot around $\eta_1 = 0$: The solid lines drawn in the left semicircle represent fixed c.m. angles χ_D, while the dashed lines in the right semicircle reflect discrete c.m. angles ξ_D. These two angles also uniquely define the dissociation kinematics; however, the advantage of the Dalitz coordinates is that the Dalitz circle is uniformly, i.e., isotropically, filled in case the kinematical phase space is exhausted randomly under no other constraints than energy and momentum conservation.

By selecting DR events with dissociation planes perpendicular to the beam direction, i.e., $|\cos(\theta)| \to 1$, the kinetic fragment energies E_i and the total kinetic energy release E reduce to the corresponding transversal energies, and (η_1, η_2) can be approximated by the corresponding transversal Dalitz coordinates (Q_1, Q_2), i.e.,

$$\eta_1 \sim Q_1 = \sqrt{\frac{M}{3m_C}} \frac{d_{H_2}^2 - d_{H_1}^2}{\sqrt{3}D^2} \tag{6}$$

and

$$\eta_2 \sim Q_2 = \frac{M m_C}{3m_H^2} \frac{d_C^2}{D^2} - \frac{1}{3}. \tag{7}$$

Strictly speaking, we measure in this way the dissociation kinematics in a plane perpendicular to the electron (molecular) beam direction. While no orientation effects are observable at $E_{c.m.} = 0$ for symmetry reasons, the flattened velocity distribution of the electron beam is in principle breaking this symmetry. Such effects, however, are expected to be small and could only recently be observed in a precision measurement of the DR of HD^+ [5].

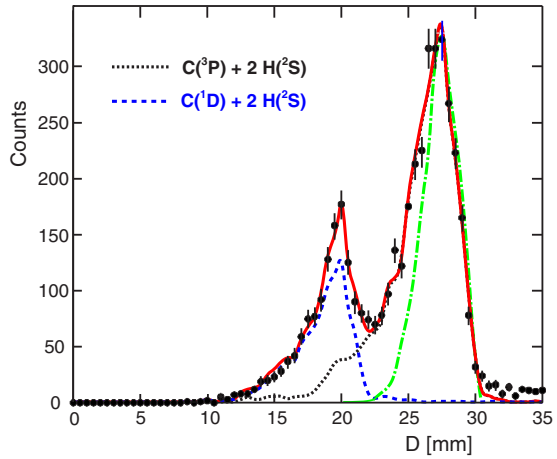

FIG. 5. (Color online) Measured projected distances D for three-fragment events observed in the DR of CH_2^+ for orientation angles $|\cos(\theta)| > 0.8$ (solid points). The solid (red) line represents the best fit of the two MC simulated distributions for the $C(^3P)$ [dotted (black) line] and the $C(^1D)$ channel [dashed (blue) line] to the measured spectrum. The dashed-dotted (green) curve shows a simulation of the projected distance distribution expected for the $C(^3P)$ channel when assuming a time resolution of $\sigma_t = 0.0$ ns.

For the finite $|\cos(\theta)|$ interval of $|\cos(\theta)| \geq 0.8$ employed in the present analysis, a given point (η_1, η_2) is expected to be smeared out in the (Q_1, Q_2) plane. However, the loss in resolution is found to be small $(\sigma_\eta \sim 0.01)$. The reason for the limited degradation of the η resolution is related to the fact that only relative energies enter into the definition of the Dalitz-coordinates; thus effects caused by the finite length of the electron target, limiting the energy resolution to about 20%, cancel out, and the broadening due to the projection of the fragment energies on the transversal plane is partly suppressed [see also Fig. 6(a)]. Under the present condition of near-zero electron collision energy, we can therefore interpret the measured (Q_1, Q_2) map as an (η_1, η_2) map of the reaction.

In order to derive the dissociation kinematics for the two three-fragment channels separately we use the proportionality of the total projected distance D to the kinetic energy release. The projected distance distribution $P(D)$ obtained under the restriction $|\cos(\theta)| \geq 0.8$ is shown in Fig. 5. The $C(^3P)$ and the $C(^1D)$ channel are clearly distinguishable and, even though the two $P(D)$ distributions have some overlap, the separation is good enough to tag the events. The distribution simulated for the $C(^3P)$ channel assuming an infinitely good time resolution (dashed-dotted curve in Fig. 5) shows that the partial overlap of the two channels is caused by the present time resolution of the 3D imaging system, while the width of the $P(D)$ distribution caused by the length of the electron target and the finite $\cos(\theta)$ interval alone would still allow for a complete channel separation. The MC calculations assuming a time resolution of $\sigma_t = 0.9$ ns, a kinetic energy release of $E_k(^3P) = 2.62$ eV, and a $[C(^3P)]:[C(^1D)]$ branching ratio of 70:30 do account very well for the observed spectrum.

The transversal Dalitz plot for the $C(^3P)$ channel was derived by considering only events with 22.5 mm $\leq D$

≤ 31.5 mm. The corresponding plot for the $C(^1D)$ channel was deduced by gating on projected distances $D < 22.5$ mm and correcting for contributions caused by the low energy tail of the $C(^3P)$ channel. The correction was performed by calculating the amount of the $C(^3P)$ contribution in the $C(^1D)$ gate using the simulated $P(D)$ spectrum for the $C(^3P)$ channel, and by subtracting the accordingly scaled $C(^3P)$-Dalitz diagram. The experimental Dalitz distributions for the two channels were symmetrized around $Q_1=0$ and efficiency corrected by dividing them by the corresponding MC simulated distributions calculated by assuming an isotropic initial (η_1, η_2) distribution. Finally, the graphs were smoothed over properly weighted next neighbor channels and normalized. The resulting transversal Dalitz distributions are displayed in Fig. 6(b) for the $C(^3P)$ and Fig. 6(c) for the $C(^1D)$ channel, respectively. For comparison, a MC simulated distribution for some (η_1, η_2) pairs, smoothed in the same way as the experimental distributions, is shown in Fig. 6(a).

The Dalitz distributions observed for the $C(^3P)$ and the $C(^1D)$ channel clearly show that the dissociation kinematics of both channels are markedly different from being isotropic and distinctly different from each other, even though the statistics of the $C(^1D)$ plot is somewhat limited. Comparison with Fig. 6(a) moreover reveals that the smoothing procedure is only slightly decreasing the resolution and is not influencing the widths of the structures observed in the experimental Dalitz plots (see Sec. IV for further discussions).

B. Energy releases

As shown by the simulated $P(D)$ distributions plotted in Fig. 5, the position of the high energy shoulder of the measured projected distance distribution for the $C(^3P)$ channel is independent of the time resolution and is well described by assuming the kinetic energy release to be $E_k(^3P)=2.62$ eV. (Note that the E_k values given are defined as the kinetic energy releases with respect to the rovibrational ground state of CH_2^+.)

For a more concisive determination of $E_k(^3P)$ we used a projected distance distribution, which was measured employing only the 2D feature of the new imaging setup, i.e., *all* molecular plane orientations are contributing. From the distribution displayed in Fig. 7, a background spectrum was subtracted, which was derived by selecting events with a c.m. distance $R_{\text{c.m.}}$ of $2\sigma_R \leq R_{\text{c.m.}} \leq 4\sigma_R$ from the beam center, and which was normalized to the measured $P(D)$ distribution at $D \geq 31$ mm; the intensity of the normalized background distribution amounted to less than a few percent at $D \ll 31$ mm. Both three-fragment channels are clearly visible in Fig. 7, but as all orientation angles θ are contributing, the projected distance distributions of the two-fragment channels are very broad, reaching from the maximum D value, determined by the total kinetic energy release and the maximum possible event distance s, down to the smallest values limited only by the minimum distinguishable light spot separation.

Fitting the upper end of the $P(D)$ distribution by MC simulated distributions for the $C(^3P)$ channel varying $E_k(^3P)$,

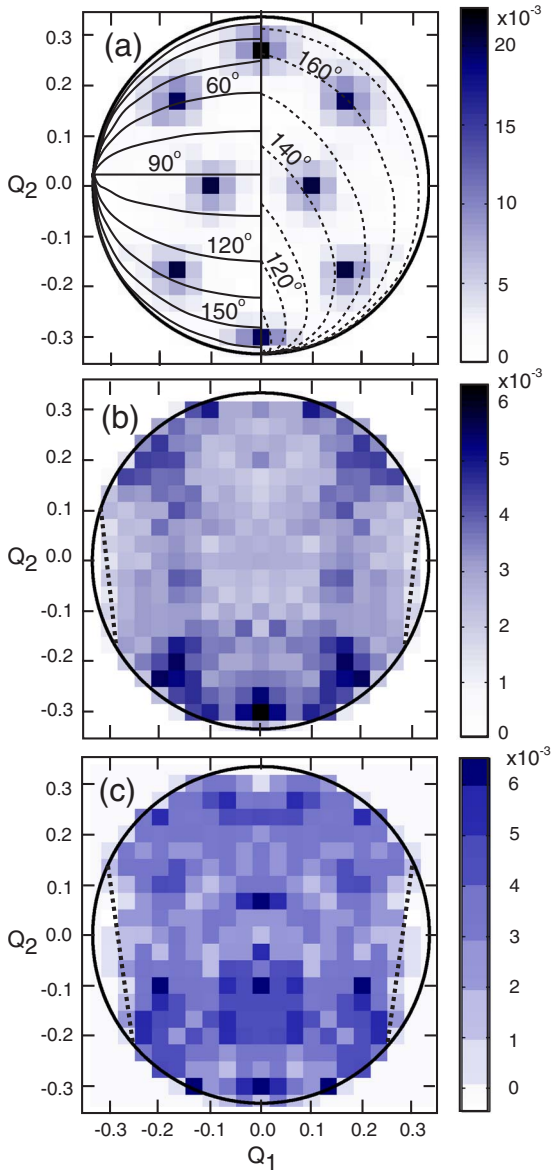

FIG. 6. (Color online) (a) MC simulated transversal Dalitz distribution for some fixed (η_1, η_2) values, displaying the resolution obtained in the present experiment. (Note that the distribution was smoothed in the same way as the experimental ones.) Also shown are the c.m. angles $\chi_D = \angle(\vec{p}_{H_1}, \vec{p}_{H_2})$ (solid lines in the left half-circle) and $\xi_D = \angle(\vec{p}_{H_>}, \vec{p}_C)$ (dashed lines in the right half-circle) for some values of χ_D and ξ_D. (b) Measured normalized transversal Dalitz distribution for the $C(^3P)$ channel, and (c) for the $C(^1D)$ channel (see also main text). Between the dotted lines and the Dalitz circle in (b) and (c) the detection efficiency was very small due to the minimum light spot distance that could be resolved in the experiment.

the kinetic energy release was determined to be

$$E_k(^3P) = (2.62 \pm 0.05) \text{ eV}.$$

The error given includes the statistical uncertainty as well as systematic contributions, the largest systematic errors being caused by our limited knowledge of the effective length of the interaction region and of the residual energy stored in the

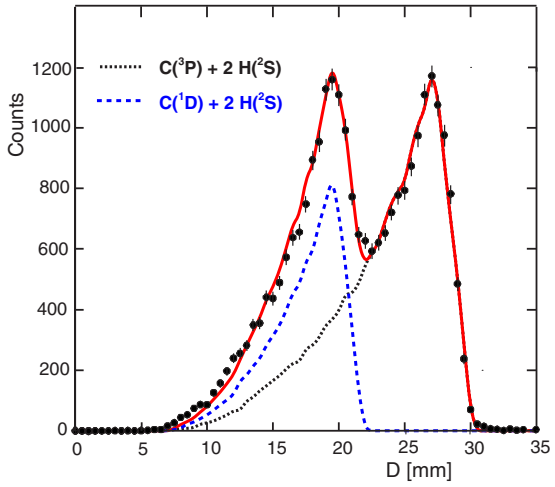

FIG. 7. (Color online) Measured projected distances D for three-fragment events observed in the DR of CH_2^+ for all orientation angles (solid points). The solid (red) line represents the best fit of the two MC simulated distributions for the $C(^3P)$ [dotted (black) line] and the $C(^1D)$ channel [dashed (blue) line] to the measured spectrum. The simulations were based on the measured Dalitz plots shown in Figs. 6(c) and 6(d).

rotational motion of the CH_2^+ ions. No dependence of the extracted E_k value on the dissociation geometry was observed. As the excitation energy of the $C(^1D)$ state relative to the $C(^3P)$ ground state of C is well known from optical investigations to be 1.264 eV [13], the $E_k(^1D)$ value is thus found to be

$$E_k(^1D) = (1.36 \pm 0.05)\ \text{eV}.$$

C. Branching ratio

The branching ratio between the two three-fragment channels was extracted from the measured projected distance distributions with and without the orientational cut.

Adjusting the MC simulated $P(D)$ histograms for the two channels to the projected distance spectrum for $|\cos(\theta)| \geq 0.8$ shown in Fig. 5, a $[C(^3P)]:[C(^1D)]$ branching ratio of 70(3):30(3) is obtained, where the error given is dominated by the systematic error due to the tail of the $C(^3P)$ peak, which depends on the time resolution. Because of the $\cos(\theta)$ cut the line shapes are not expected to be sensitive to the dissociation kinematics, and a fit using the measured instead of isotropic Dalitz distributions in the MC simulations does indeed result in the same branching ratio.

The ungated projected distance distribution shown in Fig. 7, on the other hand, can in principle depend on the details of the dissociation kinematics. To deduce the branching ratios from Fig. 7 we therefore used MC simulated $P(D)$ distributions for the two channels based on the measured Dalitz plots. The best fit to the measured distribution results in a $[C(^3P)]:[C(^1D)]$ branching ratio of 65(1):35(1), the error being the statistical error only. When using simulated distributions based on isotropic Dalitz plots, however, the quality of the fit decreased only slightly and the resulting branching ratio changed only marginally to 66(1):34(1). The branching ratio derived from the ungated projected distance distribution was found to be sensitive to the minimum distance between light spots, causing a systematic error of about ±3.

Averaging the results obtained from the analysis of the gated and ungated projected distance distribution the branching ratio is found to be

$$[C(^3P)]:[C(^1D)] = 68(4):32(4).$$

IV. DISCUSSION

Some of the results obtained in the present experiment for the three-fragment channels of the DR of $CH_2^+ + e^-$ at $E_{\text{c.m.}} \sim 0$ are at variance with the findings of Thomas *et al.* [10]: For the $[C(^3P)]:[C(^1D)]$ branching they determined a ratio of 51(4):49(5) as compared to 68(4):32(4) deduced in the present work. Moreover, for the kinetic energy release in the $C(^3P)$ channel, a value of $E_k(^3P) = 2.45$ eV was adopted by the authors, which is not only 0.17 eV smaller than the present value of $E_k(^3P) = (2.62 \pm 0.05)$ eV, but judged from Fig. 10 of Ref. [10] their assumed $E_k(^3P)$ value still seems to be too large to describe the high distance edge of their experimental projected distance distribution. In fact, the $E_k(^3P)$ value needed to reproduce the high energy edge of their transverse distance data seems to be ~0.24 eV lower than ours, while the corresponding edge of the distribution connected with the $C(^1D)$ branch would be well accounted for using the present value of $E_k(^1D) = 1.36$ eV. The reason why the $C(^3P)$ branch in the measurement reported in Ref. [10] is found to be a factor of ~2 less intense when compared to the $C(^1D)$ branch and displays a kinetic energy release which is smaller by ~10% as compared to the results of the present experiment is not obvious to us.

On the other hand, the kinetic energy release $E_k(^3P)$ deduced in the present measurement is in excellent agreement with a value that can be derived from previous photodissociation and photoionization experiments. Namely, using the ionization and dissociation energies measured in the three reactions

$$CH^2(\tilde{X}^3B_1) \rightarrow CH_2^+(\tilde{X}^2A_1) + e^-, \quad E_i,$$

$$CH_2(\tilde{X}^3B_1) \rightarrow CH(X^2\Pi) + H(^2S), \quad D_1,$$

$$CH(X^2\Pi) \rightarrow C(^3P) + H(^2S), \quad D_2,$$

with $E_i = 10.396(11)$ eV [16–18], $D_1 = 4.33(3)$ eV [16,17,19], and $D_2 = 3.465(15)$ eV [20–23], one finds $E_k(^3P) = E_i - D_1 - D_2 = 2.60(4)$ eV as compared to $E_k(^3P) = 2.62(5)$ eV derived in the present experiment. We would like to point out that also the kinetic energy release value for the $C(^1D)$ channel, which was linked to that of the $C(^3P)$ channel by the well known $^3P - ^1D$ transition energy [13], results in a very good description of the high distance edge of the projected distance distributions for this channel as shown in Figs. 5 and 7.

Based on the weighted average between this and the present value, which results in $E_k(^3P) = 2.61(3)$ eV, and the

well known dissociation energies for the hydrogen molecule of 4.478(1) eV [17] and for the $CH(X^2\Pi)$ molecule as given above, the kinetic energy releases of the two-fragment channels of the DR of CH_2^+ are found to be 7.09(3) eV for the $C(^3P)+H_2(X^1\Sigma_g)$ and 6.08(3) eV for the $CH(X^2\Pi)+H(^2S)$ branch.

In view of a still missing, quantitative model to predict branching ratios for the DR process, statistical model estimates of various sophistication have been used with differing [24], but sometimes also with quite remarkable success [25]. A simple statistical approach, which has been applied with some success to the DR of diatomic molecules [26] and also, e.g., to H_2O^+ [9], is to just consider the electronic degeneracies of the final products. This estimate, which neglects any dynamical effects, results in $[C(^3P)]:[C(^1D)]=64:36$, in excellent—although maybe fortuitous—agreement with our result, fortuitous because it is obvious from Fig. 6 that the dissociation process does depend also on the symmetry of the final states as reflected by the different dissociation kinematics observed for the two final three-fragment channels.

The Dalitz representation is especially well suited to investigating the kinematical correlation between the three final products. For a purely statistical, phase space dominated DR reaction the Dalitz plot would be evenly populated, which is noticeably not the case for the $C(^3P)$ nor for the $C(^1D)$ channel; population differences of up to a factor of 3 are observed. Two other reaction extremes are easily recognizable: First, for a *true* sequential decay via long-lived intermediate complexes the events would be located on well defined kinematical lines. In the DR of CH_2^+ a sequential decay of the excited recombination product CH_2^* can proceed via two paths involving excited H_2^* and CH^* intermediates, respectively, which should live long enough to decay outside the influence of the third particle and to be able to establish an identity, the latter time scale being governed by the rotational period of the intermediate complex, i.e., $t_{\mathrm{rot}}\sim 10^{-11}$ s. Such *true* sequential decays of CH_2^* via a well defined excited state of the intermediate system will be located in the Dalitz plot on a horizontal straight line with $\eta_2=$const for the first and on two close to vertical straight lines with $|\eta_1|\sim$const for the second path, where the respective constant is determined by the excitation energy of the intermediate complex. Second, in a *truly* prompt three-body decay, no time would be available for any rearrangements to occur, and the final state kinematic will reflect the geometrical conformation of the initial molecular ion. As the ground state of CH_2^+ is known to be bent by $\angle(\text{H-cm-H})\sim 140°$ with only a small barrier to linearity [27], we would expect the events of a prompt three-body decay of CH_2^* to occur around $\chi_D\sim 140°$ in the Dalitz plot.

A closer inspection of Fig. 6 shows that the actual decay takes place between these two extremes, although likely closer to the latter. Discussing first the $C(^3P)$ channel one notices that the main intensity, in qualitative agreement with Ref. [10], is indeed found at $\chi_D\geq 140°$, but with an energy sharing between the two hydrogen atoms expected in case the dissociation would start with a symmetric, leading to $\eta_1\sim 0$, and an antisymmetric stretching vibration, resulting in $\eta_1\sim\pm 0.2$. A less pronounced maximum in the Dalitz plot of $C(^3P)$ is observed at $(\eta_1,\eta_2)\approx(\pm 0.20,+0.20)$, which corresponds to $\chi_D\sim 45°$ and an asymmetric energy sharing between the two H atoms, a decay geometry which does require a considerable angular rearrangement of the hydrogen atoms during dissociation. Unlike the $C(^3P)$ branch, the $C(^1D)$ channel seems to prefer equal energy sharing between the two hydrogen atoms. Moreover, for the main intensity group the angle between the two hydrogen momenta is smaller, i.e., $\chi_D\sim 110°-135°$, and decays with $\chi_D\leq 90°$ seem to be more likely than for the $C(^3P)$ channel.

Minaev and Larsson [28] calculated in a one-dimensional approach potential energy curves for the excited methylene molecule CH_2^* along the linear and the bent reaction coordinates in an attempt to identify the dissociative potential energy curves leading to the three-body dissociation channel. Their main conclusion is that only the 3^3A_2 state, which correlates with the $1^3\Sigma_u^-$ state in the linear conformation and which is energetically very close to the dissociation energy, can be responsible for the three-fragment channels in the DR of CH_2^+. Moreover, they argue that the 3^3A_2 state will dissociate to the $C(^3P)$ channel at linear structure and to the $C(^1D)$ channel for bond angles around $\angle(\text{H-cm-H})=132°$. These conjectures are in qualitative agreement with our findings for the most likely decay pattern. For a more detailed analysis, however, the two-dimensionality of the molecule has to be taken into account for a proper description of the interactions between the various potential energy surfaces and of the dynamics of the process.

V. CONCLUSIONS

Using a 3D-imaging technique, we provide unique kinematic information for the three-body breakup of the methylene ion after dissociative recombination. Selecting events with dissociation planes perpendicular to the beam direction we were able to construct the individual Dalitz plots for the two three-fragment channels and thereby to investigate and to highlight the different dissociation geometries. Furthermore, the branching ratio between the two channels and the kinetic energy release could be determined. The new 3D-imaging technique is found to be well suited to studying the dissociation dynamic of the complete breakup channels in the DR of polyatomic molecular ions.

ACKNOWLEDGMENTS

D.S. acknowledges support from the Joseph Meyerhoff Trust, granted by the Weizmann Institute of Science. The work was supported by the Israel Science Foundation and by the German Israel Foundation for Scientific Research (GIF) under Contract No. I-707-55.7/2001.

[1] D. R. Bates, Phys. Rev. **78**, 492 (1950).
[2] See, e.g., A. I. Florescu-Mitchell and J. B. A. Mitchell, Phys. Rep. **430**, 277 (2006) and references therein.
[3] V. Kokoouline and C. H. Greene, Phys. Rev. A **68**, 012703 (2003).
[4] E. Herbst and W. Klemperer, Astrophys. J. **185**, 505 (1973); E. Herbst, Philos. Trans. R. Soc. London, Ser. A **358**, 2523 (2000).
[5] S. Novotny *et al.* (unpublished).
[6] D. Strasser, X. Urbain, H. B. Pedersen, N. Altstein, O. Heber, R. Wester, K. G. Bhushan, and D. Zajfman, Rev. Sci. Instrum. **71**, 3092 (2000).
[7] D. Strasser, L. Lammich, S. Krohn, M. Lange, H. Kreckel, J. Levin, D. Schwalm, Z. Vager, R. Wester, A. Wolf, and D. Zajfman, Phys. Rev. Lett. **86**, 779 (2001); D. Strasser, L. Lammich, H. Kreckel, S. Krohn, M. Lange, A. Naaman, D. Schwalm, A. Wolf, and D. Zajfman, Phys. Rev. A **66**, 032719 (2002); D. Strasser, L. Lammich, H. Kreckel, M. Lange, S. Krohn, D. Schwalm, A. Wolf, and D. Zajfman, *ibid.* **69**, 064702 (2004).
[8] Å. Larson, A. Le Padellec, J. Semaniak, C. Strömholm, M. Larsson, S. Rosén, R. Peverall, H. Danared, N. Djuric, G. H. Dunn, and S. Datz, Astrophys. J. **505**, 459 (1998).
[9] R. Thomas, S. Rosén, F. Hellberg, A. Derkatch, M. Larsson, S. Datz, R. Dixon, and W. J. van der Zande, Phys. Rev. A **66**, 032715 (2002).
[10] R. D. Thomas, F. Hellberg, A. Neau, S. Rosén, M. Larsson, C. R. Vane, M. E. Bannister, S. Datz, A. Petrignani, and W. J. van der Zande, Phys. Rev. A **71**, 032711 (2005).
[11] F. Sprenger, M. Lestinsky, D. A. Orlov, D. Schwalm, and A. Wolf, Nucl. Instrum. Methods Phys. Res. A **532**, 298 (2004).
[12] A. Baer, M. Grieser, L. Knoll, J. Levin, R. Repnow, D. Schwalm, Z. Vager, R. Wester, A. Wolf, and D. Zajfman, Phys. Rev. A **59**, 1865 (1999).
[13] N.I.S.T. Atomic Database, www.physics.nist.gov/PhysRevData/ASD/
[14] P. Jensen, M. Brumm, W. P. Kraemer, and P. R. Bunker, J. Mol. Spectrosc. **172**, 194 (1995).
[15] R. H. Dalitz, Philos. Mag. **44**, 1068 (1953).
[16] H. Prophet, J. Chem. Phys. **38**, 2345 (1963).
[17] G. Herzberg, *Electronic Spectra and Electronic Structure of Polyatomic Molecules*, reprint edition, Molecular Spectra and Molecular Structure (Krieger, New York, 1991), Vol. III, p. 583.
[18] M. Litorja and B. Ruscic, J. Chem. Phys. **108**, 6748 (1998).
[19] D. G. Leopold, K. K. Murray, A. E. S. Miller, and W. C. Lineberger, J. Chem. Phys. **83**, 4849 (1985).
[20] G. Herzberg, *Spectra of Diatomic Molecules*, reprint edition, Molecular Spectra and Molecular Structure (Krieger, New York, 1989), Vol. I, pp. 459, 518, and 530.
[21] R. G. Brewer and F. L. Kester, J. Chem. Phys. **40**, 812 (1964).
[22] H. Helm, P. C. Cosby, M. M. Graff, and J. T. Moseley, Phys. Rev. A **25**, 304 (1982).
[23] Z. Amitay, D. Zajfman, P. Forck, U. Hechtfischer, B. Seidel, M. Grieser, D. Habs, R. Repnow, D. Schwalm, and A. Wolf, Phys. Rev. A **54**, 4032 (1996).
[24] E. T. Galloway and E. Herbst, Astrophys. J. **376**, 531 (1991) and references cited therein.
[25] D. Strasser, J. Levin, H. B. Pedersen, O. Heber, A. Wolf, D. Schwalm, and D. Zajfman, Phys. Rev. A **65**, 010702(R) (2001).
[26] W. J. van der Zande, in *Proceedings of the 1999 Conference on Dissociative Recombination: Experiment and Application*, edited by M. Larsson, J. B. A. Mitchell, and I. F. Schneider (World Scientific, Singapore, 2000), p. 251.
[27] G. Osmann, P. R. Bunker, W. P. Kraemer, and P. Jensen, Chem. Phys. Lett. **309**, 299 (1999); L. Lammich, H. Buhr, H. Kreckel, S. Krohn, M. Lange, D. Schwalm, R. Wester, A. Wolf, D. Strasser, D. Zajfman, Z. Vager, I. Abril, S. Heredia-Avalos, and R. Garcia-Molina, Phys. Rev. A **69**, 062904 (2004).
[28] B. Minaev and M. Larsson, Chem. Phys. **280**, 15 (2002).